Mainstream Aerodynamic Effects Due to Wheelspace Coolant Injection in a High-Pressure Turbine Stage: Part I—Aerodynamic Measurements in the Stationary Frame

Christopher McLean[1]
e-mail: cmclean@techkor.com

Cengiz Camci
Professor of Aerospace Engineering.
e-mail: cxc11@psu.edu

Turbomachinery Heat Transfer Laboratory,
The Pennsylvania State University,
University Park, PA 16802

Boris Glezer[2]
Consultant,
San Diego, CA 90909
e-mail: bglezer@san.rr.com

The relative aerodynamic and performance effects associated with rotor–NGV gap coolant injections were investigated in the Axial Flow Turbine Research Facility (AFTRF) of the Pennsylvania State University. This study quantifies the effects of the coolant injection on the aerodynamic performance of the turbine for radial cooling, impingement cooling in the wheelspace cavity and root injection. Overall, it was found that even a small quantity (1 percent) of cooling air can have significant effects on the performance character and exit conditions of the high pressure stage. Parameters such as the total-to-total efficiency, total pressure loss coefficient, and three-dimensional velocity field show local changes in excess of 5, 2, and 15 percent, respectively. It is clear that the cooling air disturbs the inlet end-wall boundary layer to the rotor and modifies secondary flow development, thereby resulting in large changes in turbine exit conditions. [DOI: 10.1115/1.1401026]

Introduction

Gas turbine systems are rapidly becoming one of the primary sources for electrical power generation throughout the world. The United States Department of Energy estimates that over the next 20 years, as much as half of the new power generating capacity added in the United States will be from gas turbine systems [1]. Improvements to gas turbine technology can take many forms, including lower specific fuel consumption/improved efficiency, better specific power, increased durability and service life, and lower acoustic noise, smoke, and gaseous emissions [2]. A direct result of the desire to increase gas turbine efficiency and specific power output is an increase in the required turbine entry temperature (TET) and overall pressure ratio. Modern engines operate well below theoretical limits. The stoichiometric combustion limit for turbine inlet temperature is approximately 2000°C, while modern metallurgy only allows surface temperatures of approximately 1000°C [3]. Aggressive air-cooling of turbine blades, platforms, and wheelspaces allows turbine inlet temperatures of 1450°C. However, cooling penalties can easily offset the benefits of the increasing TET. Energy is required to compress and pump the cooling air to the turbine blades and wheelspace, and cooling air bled from the compressor bypasses the combustion chamber so the full work potential is never realized. Overall turbine cycle efficiency is lowered in the process. In addition, when mixing cooling air with the mainstream gas, significant turbulence is generated and the end-wall rotor boundary layers are disturbed affecting the secondary flow. Enthalpy and stagnation pressures are lost, lowering the turbine stage efficiency. An effective turbine design must account for all of these factors.

A major concern in modern gas turbine engines is the cooling of turbine wheelspace. The complexity of a modern high-pressure turbine wheelspace is depicted in Fig. 1 [4]. Many present day gas turbine engines operate with mainstream gas temperatures exceeding 1450°C in the high-pressure turbine stage. Turbine designers need to give special attention to the cooling of turbine wheelspaces. Turbine wheelspaces contain rotor bearings and are constructed from lower temperature metals than turbine blades. Allowing the high-temperature gas from the mainstream to be ingested would significantly reduce turbine life. In a gas turbine engine, the spinning rotor disk induces periodic outward flow on the rotor side of the wheelspace that is counteracted by flow ingestion on the stationary side of the wheelspace [5,6]. This circulation leads to the ingestion of hot mainstream gases, and acts to raise the internal temperature of the wheelspace materials significantly. To counter this effect, cooling air is pumped into the wheelspace cavity. This continuous supply of cool air keeps internal components within thermal limits. However, the pumping of the wheelspace coolant and its eventual mixing with the mainstream boundary layer flow causing performance degradation.

Much literature exists on the aerodynamics of rotating disks and the heat transfer effects of cooling within the wheelspace cavity. Theodore von Karman [7] first reported the theoretical flow field for an infinite rotating disk in an infinite medium. Early works on wheelspace aerodynamics and wheelspace cooling include Cobb and Saunders [8], Maroti [9], Daily and Nece [10] and Dorfman [11]. Cobb and Saunders obtained data on rotor-averaged heat transfer coefficients, while Maroti demonstrated that the outflow from a rotating disk is periodic in nature. Daily and Nece studied the effects of cavity spacing on disk torque. Metzger et al. [12] presented experimental data for impingement flow onto a rotating disk. Later works by Popiel and Boguslawski [13], and Qureshi [14] obtained radial section-averaged rotor heat transfer information. Pincombe [15] performed detailed flow visualization studies with rotational and stationary disk combinations to study the highly three-dimensional secondary flow present in the wheelspace cavity. More recent studies such as those per-

[1]Present address: Division Manager, Techkor Instrumentation, A Division of ACT, Inc., Harrisburg, PA.

[2]Former Head of ''Turbine Cooling Design and Analysis'' at Solar Turbines, Inc., San Diego, CA.

Contributed by the International Gas Turbine Institute and presented at the 46th International Gas Turbine and Aeroengine Congress and Exhibition, New Orleans, Louisiana, June 4–7, 2001. Manuscript received by the International Gas Turbine Institute February 2001. Paper No. 2001-GT-119. Review Chair: R. Natole.

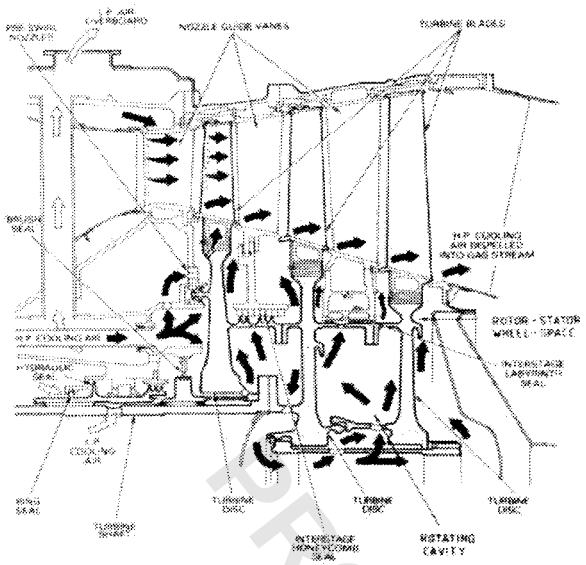

Fig. 1 Wheelspace coolant flow in a high-pressure turbine stage showing the complexity of the internal wheelspace and the mixing of the coolant flow with the mainstream flow, [4].

formed by Bunker [5,6] describe the detailed two-dimensional heat transfer patterns within turbine wheelspaces.

Published research neglects to study the secondary aerodynamic effects of wheelspace coolant mixing with the mainstream flow and its effects on platform heat transfer. Due to the fact that wheelspace coolant is injected upstream of the rotor blade throat, it will incur lower losses than film cooling injected after the throat. The wheelspace coolant has potential for endwall cooling given the proper geometry. The question remains as to the aerodynamic penalties of wheelspace coolant injected into the mainstream and its influence on turbine stage performance.

Endwall cooling studies can lend some understanding to the effect of wheelspace coolant injection. Both affect the rotor inlet boundary layer, pressure field, and the consequent vortex development. In film cooling, higher blowing ratios lead to higher losses due to increased shear and increased rotationality of the flow. Highly three-dimensional flow along the end wall interacts with the cooling flows. Passage vortices, boundary layers, shock waves, and horseshoe vortices all play a significant role.

Turbine designers require three important pieces of information in the design of cooled high-pressure turbines when active wheelspace cooling is required.

1 The cooling air should be injected in such a manner that the wheelspace is cooled below critical material temperatures. Much information exists in the form of empirical relationships.

2 The cooling air cannot cause excessive performance losses. If the losses due to the cooling are too high, they will negate any gains from increasing the turbine entry temperature. Overcooling causes windage losses due to rotational drag within the wheelspace and causes aerodynamic losses when mixed with the mainstream flow. The use of seals and jet preswirl greatly reduces the amount of cooling flow required and its associated losses. Little information exists on the mixing of the wheelspace cooling air with the mainstream flow and its associated losses.

3 The wheelspace cooling injected into the mainstream affects the rotor endwall heat transfer. Some information exists on platform cooling related to wheelspace cooling gap injection.

However, most of the research on platform cooling is focused on film cooling. Research has neglected the effects of the wheelspace cooling flow's interaction with the mainstream and the effects of modifying/disturbing the rotor end-wall boundary layer. This area is the subject of continued research.

Experimental Test Facility

The Axial Flow Turbine Research Facility (AFTRF) is a continuous flow open loop facility 0.916 m in diameter with an advanced axial turbine blading configuration (Fig. 2). The research facility is located at the Pennsylvania State University's Center for Gas Turbines and Power. The facility consists of a bellmouth inlet, a single high-pressure turbine stage with a nozzle guide vane assembly and rotor, and outlet guide vanes. The facility was used for the current research program with significant modifications to allow for wheelspace cooling. Table 1 lists the critical design and operating data for the AFTRF.

The AFTRF is powered by four stages of adjustable pitch axial flow fans. A detailed description of the AFTRF can be found in Lakshminarayana et al. [16]. An aerodynamically designed exit throttle is used to adjust the pressure rise across the stage. The

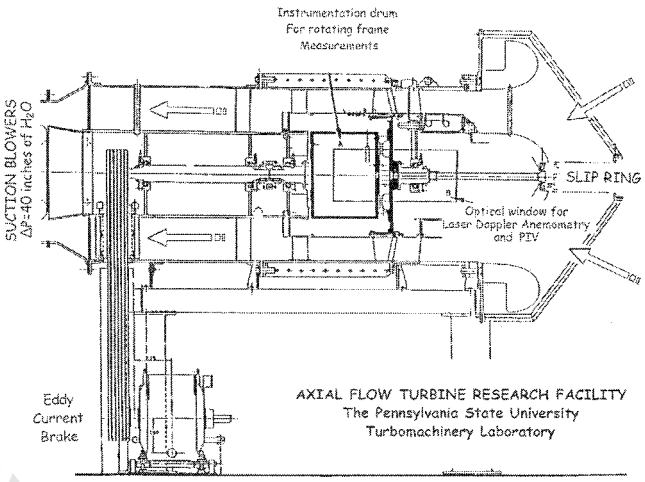

Fig. 2 Axial flow Turbine Research Facility of the Pennsylvania State University

Table 1 AFTRF critical data

AFTRF Parameter	Value	AFTRF Parameter	Value
Power	60.6 kW	Tip Radius	0.4582 m
Design RPM	1322	Tip Clearance	0.762 mm
Midspan Blade Speed (U_m)	54.89 m/s	Hub to Tip Ratio	0.7269
Design Mass Flow	11.05 kg/s	Rotor Chord Length	0.1287 m
Total-to-Total Efficiency	0.893	Rotor Spacing	0.1028 m
Nozzle Efficiency	0.994	Rotor Maximum Thickness	22.0 mm
Rotor Efficiency	0.882	Rotor Turning Angle	95° at Tip 126° at Hub
Pressure Ratio (P_{04}/P_{05})	1.078	Nozzle to Rotor Spacing	20%
Temperature Ratio (T_{05}/T_{04})	0.981	Number of Nozzle Vanes	23
Pressure Drop	56.04 mm Hg	Nozzle Turning Angle	70°
Inlet Re for Nozzle	3-4 x 10^5	Nozzle Chord Length	0.1768 m
Inlet Re for Rotor	3-5 x 10^5	Nozzle Spacing	0.1308 m
Number of Rotor Blades	29	Nozzle Maximum Thickness	38.8 mm
Hub Radius	0.3331m		

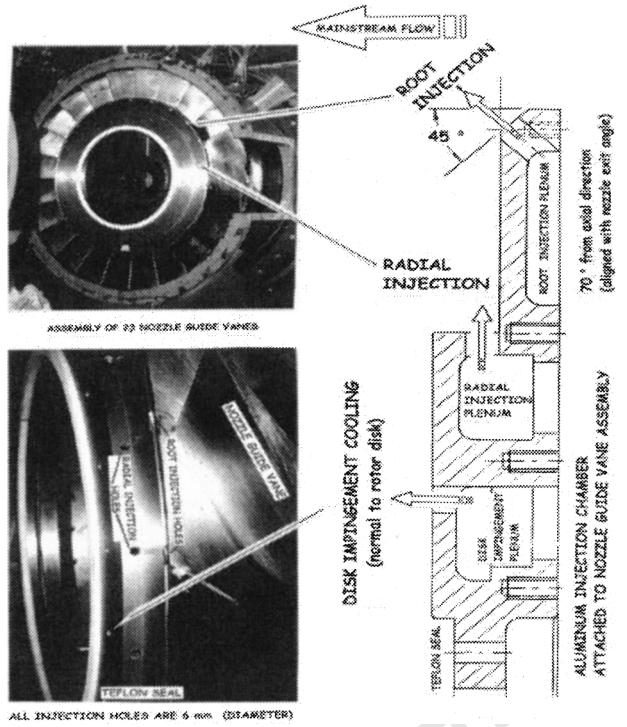

Fig. 3 Cooling flow injection chambers for radial cooling, impingement cooling, and root injection

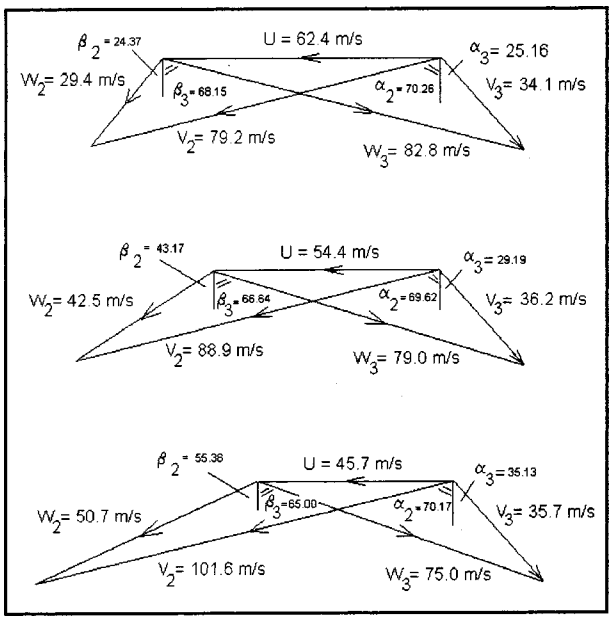

Fig. 4 Velocity triangles for the rotor at the hub (r = 0.3353 m), midspan (r = 0.3998 m), and tip (r = 0.4583 m)

four fans in series produce a pressure drop for the turbine test section of 74.7 mm Hg with a volumetric flow of 10.4 m^3/s (11.4 kg/s). A water-cooled eddy current brake dissipates the power generated by the turbine rotor. The speed of the rotor is fully adjustable from 175 to 1695 rpm and is stable to within ± 1 rpm. The operating point reference of 1322 rpm is at an ambient temperature and pressure of 25°C and 98.5 kPa, respectively. Operating the facility at corrected rotor speed minimizes effects of daily variations in inlet temperature conditions.

A major modification to the original AFTRF design was made to accommodate the injection of cooling air to the turbine wheelspace. Three independent sets of 23 cooling holes and plenums were added evenly spaced around the circumference. All cooling holes had a diameter of 6 mm.

Each set of 23 cooling holes is fed with a separate plenum and could be individually operated. All cooling holes are located around the circumference at the 23 nozzle trailing edge locations. Set I (radial cooling) injects cooling air radially along the nozzle wheelspace disk, Set II (impingement cooling) injects cooling air normal to the rotor disk, and Set III (root injection) injects cooling air at the nozzle guide vane root along the exit angle inclined 45 deg to the hub surface and aligned with the exit flow angle. The geometry of the three cooling hole sets is shown in Fig. 3. The cooling flow parameters are summarized in Table 2 where the mass flow ratio was defined as $\dot{m}_C/\dot{m}_P$, the mean discharge velocity was defined as $U_C = \dot{m}_C/n\rho A$, the mean discharge Mach number was defined as $M = U_C/\sqrt{\gamma RT_C}$, the blowing rate was defined as $\rho_C U_C/\rho_P U_P$ and the velocity ratio was defined as U_C/U_P.

Table 2 Coolant flow parameters for stationary frame measurements

Mass Flow Ratio $\dot{m}_C/\dot{m}_P$	Mean Discharge Velocity $U_C = \dot{m}_C/n\rho A$	Mean Discharge Mach Number $M = U_C/\sqrt{\gamma RT_C}$	Blowing Rate $\rho_C U_C/\rho_P U_P$	Velocity Ratio U_C/U_P
1.00%	158 m/s	0.46	1.56	3.95
1.25%	198 m/s	0.58	1.96	4.95
1.50%	237 m/s	0.70	2.35	5.93

The scaling of the various cooling flow parameters were established by considering the operational conditions of modern turbines. Blowing rates available in the AFTRF agree well with those in the literature.

Measurements

Exit flow surveys were taken in the AFTRF with and without cooling injection (1 percent) in the stationary frame. The flow field was measured using both five-hole and modified Kiel probes. The modified Kiel probe contained a miniature thermocouple in the stagnation tube. The probes were installed 1.5 axial chords downstream of the rotor. Probes were traversed in the radial and circumferential directions (stationary $r-\Theta$ traverse). Consequently, all rotor-induced variations in the circumferential direction were averaged out.

The cooled and noncooled data were taken in an interlaced manner. At each measurement point in the traverse grid, the probe readings were recorded with and without cooling flow. A set of high-speed solenoids controlled the coolant flow. This method ensured that the cooled and noncooled cases experienced the same mainstream flow conditions. Small variations in mainstream flow would otherwise be misreported as changes due to the cooling flow.

The pressures and temperatures sensed by the five-hole and Kiel probes were sampled via a personal computer with an analog to digital converter card. Cooled and noncooled data ($P_{05,1}, P_{05,2}, P_{05,3}, P_{05,4}, P_{05,5}$ for the five-hole probe and P_{05}, T_{05} for the Kiel probe) were sampled at 100 Hz for 15 seconds at each measurement point. The resulting data were time averaged at each measurement point and proper calibration equations were applied. The measured data at this sampling rate and duration were statistically stable. The result were data sets for cooled and noncooled cases containing T_0, P_0, P_S, u, v, w, U, a, and b at the rotor exit in (r, θ) plane.

Loading Coefficient. The loading coefficient gives insight into the total pressure drop across the turbine stage. The loading coefficient is defined as

Table 3 Percentage change in total pressure coefficient due to 1 percent cooling flow (passage-averaged)

$\Psi = \frac{P_{04} - P_{05}}{\frac{1}{2}\rho U_m^2}$	Radial Cooling Percentage Change	Impingement Cooling Percentage Change	Root Injection Percentage Change
Minimum	-1.50	-0.73	-2.57
Maximum	1.70	0.86	1.46
Average	-0.013	-0.067	-0.307

Table 4 Percentage change in static pressure coefficient due to 1 percent cooling flow (passage-averaged)

$\Psi_s = \frac{P_4 - P_5}{\frac{1}{2}\rho U_m^2}$	Radial Cooling Percentage Change	Impingement Cooling Percentage Change	Root Injection Percentage Change
Minimum	-0.18	0.00	-0.65
Maximum	0.31	0.30	0.29
Average	0.067	0.079	-0.126

$$\Psi = \frac{P_{04} - P_{05}}{1/2\rho U_m^2} \tag{1}$$

and the static pressure loss coefficient is defined as

$$\Psi_s = \frac{P_4 - P_5}{1/2\rho U_m^2} \tag{2}$$

where P_4 and P_{04} are the wall static pressure and midstream total pressure at location 4, respectively. Earlier measurements from Lakshminarayana et al. [17] showed these values to be representative of the inlet mass averaged values. The total and static pressure loss coefficients shown in Figs. 6 and 7 are simultaneously measured with a five-hole probe. The data with "no cooling" are displayed with the viewer looking upstream into the stage at location 5. Viewing direction is normal to the plane of data. The loss coefficients show significant radial and circumferential variations. Strong remnants of the nozzle wake and nozzle passage vortices are visible in the data shown in Figs. 6 and 7. Near the tip ($r = 0.44$) the loss coefficient is observed to be lower, showing the underturning due to leakage flow. Near the midspan ($r = 0.38$), a small region of overturning is visible.

The effect of the cooling injection can be seen qualitatively in the pressure coefficient data. The 1 percent cooling flow is able to cause significant local perturbations. Root injection shows the largest magnitude changes followed by radial cooling, and impingement cooling. In all cases the strongest effects are below midspan, but dwindling effects exist out to the tip regions. The magnitude changes in the total pressure coefficient were more significant that the static pressure coefficient.

All three cooling methods caused significant local changes and a general redistribution of the pressure coefficient data over the entire passage in both radial and tangential directions. Maximum effects ranged from 1.70, 0.86, and 2.57 percent for radial cooling, impingement cooling, and root injection, respectively.

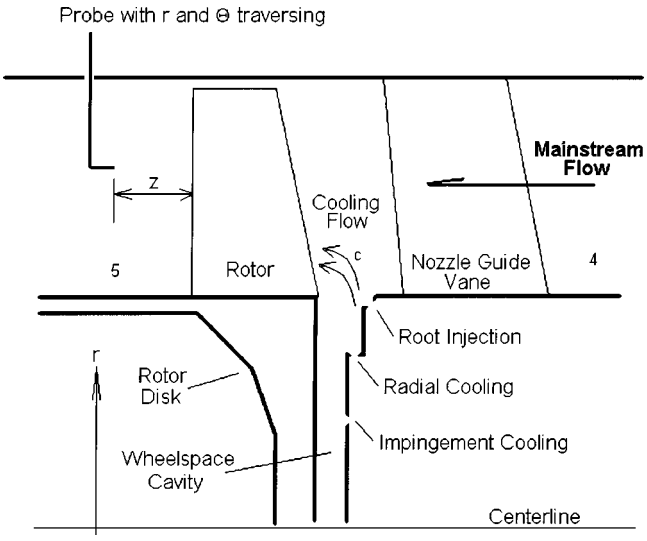

Fig. 5 Five-hole probe location in the stationary frame

Although the local perturbations were quite high, when passage average data were evaluated the changes were found to be significantly smaller. Radial and impingement cooling showed little overall effect on the pressure coefficient. The main result of radial and impingement cooling was a redistribution of pressure coefficient data. Root injection was able to affect the overall pressure coefficient as well as cause a redistribution of pressure coefficient data. The amount of change was almost five times that of impingement cooling and 30 times that of radial cooling. Passage averaged percentage changes in total pressure loss for radial cooling, impingement cooling, and root injection are −0.013, −0.067, and −0.307 percent, respectively. Summary data are presented in Table 3.

The decreases found in the pressure loss data are similar to that found by Friedrichs [18] in an endwall cooling study. He states that by neglecting the losses in the cooling lines, the change in overall loss is small for endwall cooling and can be positive or negative depending on the coolant supply pressure. Friedrichs further found that ejection of coolant ahead of the lift off lines could significantly change the secondary flow and reduce the associated losses.

Static pressure coefficients showed little effect from the cooling. Passage averaged percentage changes in static pressure loss for radial cooling, impingement cooling, and root injection are 0.067, 0.079, and −0.126 percent, respectively. Summary data are presented in Table 4.

Velocity Components and Exit Angles. The change in the individual velocity components due to wheelspace coolant injection can be observed best by examining the passage-averaged velocity components. Circumferentially averaged velocity components in radial, tangential, and axial directions are obtained from a

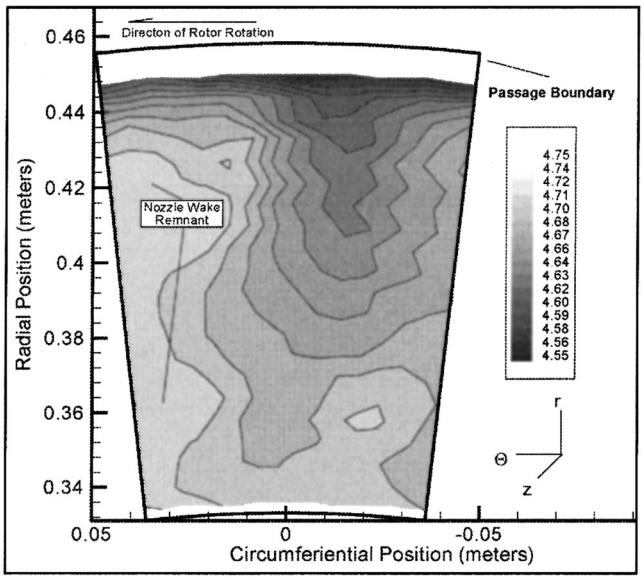

Fig. 6 Static pressure loss coefficient, 1.5 axial chords downstream of the rotor exit looking upstream from location 5

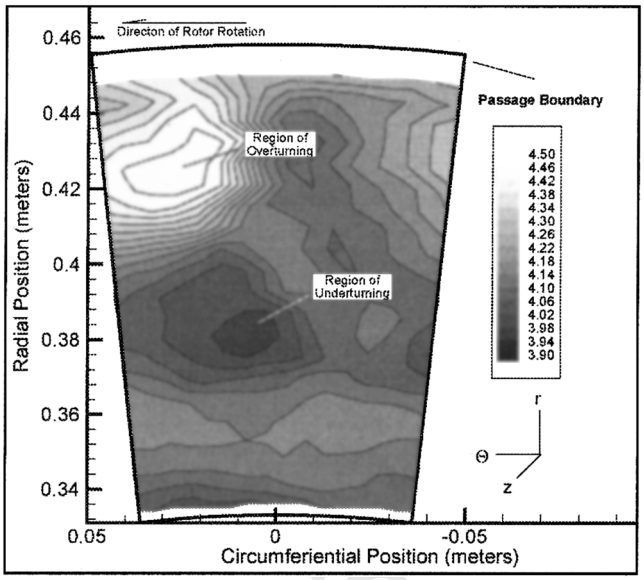

Fig. 7 Total pressure loss coefficient, 1.5 axial chords downstream of the rotor exit looking upstream from location 5

Table 5 Percentage change in total-to-total efficiency due to cooling flow (mass-averaged)

Mass Flow Ratio	Radial Cooling	Impingement Cooling	Root Injection
1.00%	+0.187	-0.777	+1.524
1.25%	-0.359	-0.248	+2.062
1.50%	+0.242	-0.149	+3.129

Table 6 Uncertainty in fundamental quantities

Parameter	Precision Error (S_x)	Bias Error (B_x)
u, v, w	0.4%	1.9%
Um	0.08%	0.4
Po, Ps	0.015%	0.2%
To	0.1 K	0.25 K
ρ	0.16%	2.0%

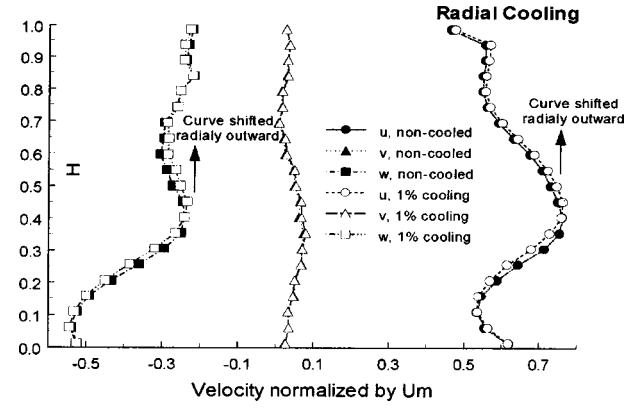

Fig. 8 Change in normalized, passage averaged, velocity components (u,v,w) due to 1 percent radial cooling. Stationary frame, 1.5 chords downstream.

subminiature five hole probe mounted 1.5 chord downstream of the rotor trailing edge plane, as shown in Fig. 5. Aerodynamic measurement details of this probe can be found in Wiedner [19]. The velocity data normalized by U_m and exit angles are displayed in Figs. 8–13. The radial velocity component (v) shows little

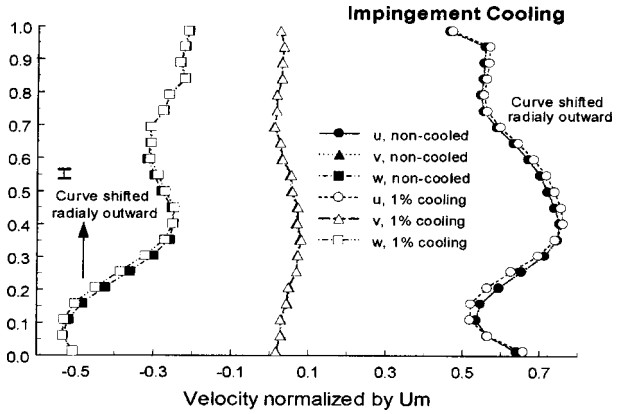

Fig. 9 Change in normalized, passage averaged, velocity components (u,v,w) due to 1 percent impingement cooling. Stationary frame, 1.5 chords downstream.

effect due to the coolant injection. In all three cases this velocity remains small and unperturbed. The effects of coolant inject are best observed in the axial (u) and tangential (w) components. The root injection shows the largest changes.

The baseline velocity distribution shows significant areas of overturning and underturning. Overturning and underturning refer to the deviation of the flow exit angle from invicid design. In a

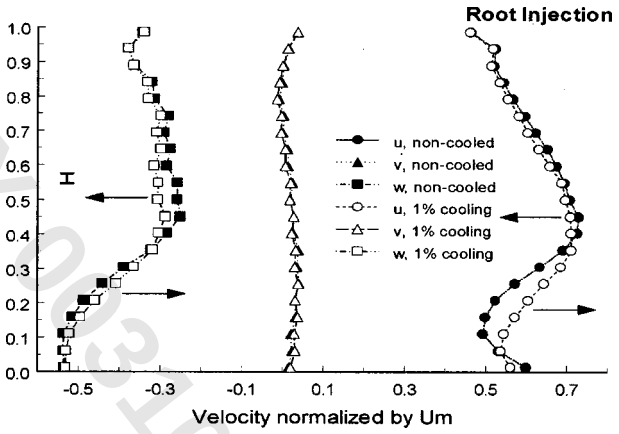

Fig. 10 Change in normalized, passage averaged, velocity components (u,v,w) due to 1 percent root injection. Stationary frame, 1.5 chords downstream.

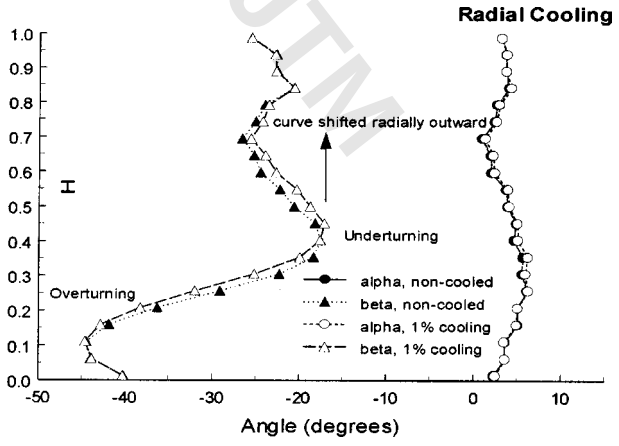

Fig. 11 Change in pitch (α) and yaw (β) angles due to 1 percent radial cooling. Stationary frame 1.5 chords downstream.

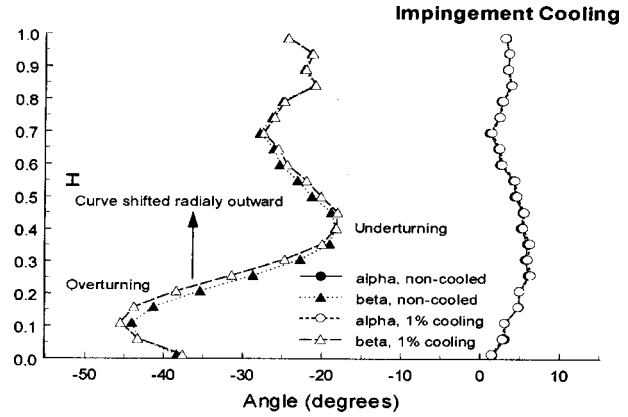

Fig. 12 Change in pitch (α) and yaw (β) angles due to 1 percent impingement cooling. Stationary frame, 1.5 chords downstream.

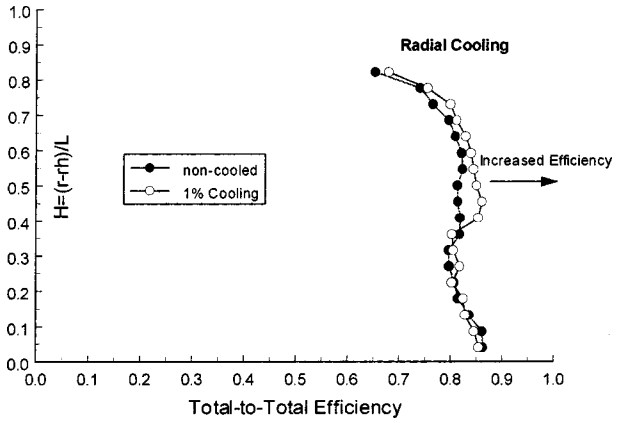

Fig. 14 Change in total-to-total efficiency (η) due to 1 percent radial cooling

real viscous fluid, the turbine passage has significant secondary flows in the form of vortices. These vortices will locally underturn or overturn the flow. An inviacid analysis of the AFTRF turbine stage yields an exit angle of approximately −30 deg. It can be seen that at an H of 0.1 a region of overturning exists and at an H of 0.4 a region of underturning exists. This flow profile is typical for the AFTRF and was first documented by Zaccaria [20].

Radial cooling shifts the velocity profiles radially outward. The overall magnitude of axial and tangential velocity is unchanged however, the point of maximum overturning is shifted radially by $H=0.10$. This can best be seen in the exit angle measurements (Fig. 17). This would seem to indicate that the vortex location is being modified but that the strength is not. Friedrichs [18] has also observed that endwall platform cooling could significantly shift the location of the passage vortex but that the strength was not significantly affected. The radial cooling is injected normal to the mainstream flow and would energize the rotor inlet boundary layer. This energizing would thicken the inlet rotor boundary layer. The thicker boundary layer would displace the core flow and the passage vortex slightly toward the tip region.

The impingement cooling shows similar effects to the radial cooling. Again, the overall magnitude of axial and tangential velocity is unchanged. The point of maximum overturning is shifted radially by $H=0.05$ smaller than with radial cooling. The impingement cooling enters the mainstream flow with minimal momentum having been stagnated on the rotor disk. The boundary layer would be thickened, but not to the degree found with radial cooling. The thicker boundary layer would displace the core flow and the passage vortex slightly toward the tip region.

The root injection shows the most significant effects due to the coolant injection and is fundamentally different from radial cooling and impingement cooling. Root injection has the ability to affect the magnitude of the overturning and underturning. The root injection energizes the nozzle wake and boundary layer near the hub wall. With an injection hole size on the order of the trailing edge thickness and with the injection inclined at 45 deg to the hub wall, the root injection can significantly energize the wake region. This has the effect of reducing the passage vortex and reducing the magnitude of overturning and underturning. Friedrichs et al. [18] also observed that significant cooling injection could delay the three-dimensional separation of the inlet boundary layer thereby reducing the strength of the passage vortex.

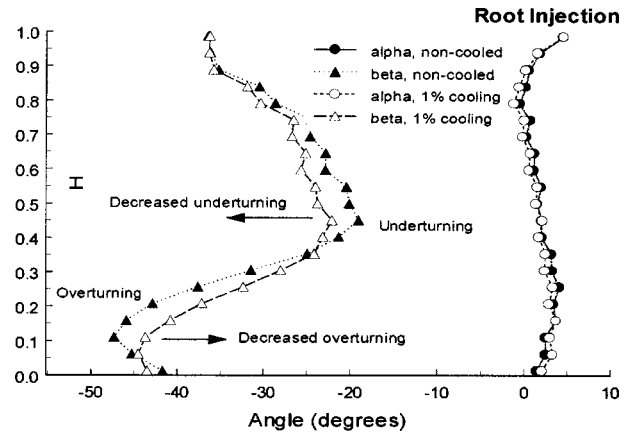

Fig. 13 Change in pitch (α) and yaw (β) angles due to 1 percent root injection. Stationary frame, 1.5 chords downstream.

Total-to-Total Efficiency. Considering the primary flow (nozzle inlet to rotor exit) and one cooling stream (cooling inlet to rotor exit), the total-to-total efficiency can be written as:

$$\sigma_{tt,c}=\frac{1+\left(\frac{\dot{m}_c}{\dot{m}_p}\right)\left(\frac{T_{oc}}{T_{04}}\right)-\left(\frac{\dot{m}_c}{\dot{m}_p}+1\right)\left(\frac{T_{05}}{T_{04}}\right)}{1+\left(\frac{\dot{m}_c}{\dot{m}_p}\right)\left(\frac{T_{oc}}{T_{04}}\right)-\left(\frac{\dot{m}_c}{\dot{m}_p}+1\right)\left(\frac{P_{05}}{P_{04}}\right)^{(\gamma-1)/\gamma}} \quad (3)$$

The specific efficiency equation suggested by McDonel and Eiswerth [21] is for total-to-total stage efficiency. Pumping work is not included in the stage efficiency equation. Pumping work losses are better handled in cycle analysis.

Measurements were taken at three blowing rates (1.00, 1.25, and 1.50 percent). Passage-averaged efficiency data are shown with their respective P_{05}/P_{04} and T_{05}/T_{04} in Figs. 21–29. Data are shown for 1 percent cooling only.

Cooling flows were able to modify the magnitude of the total pressure and total temperature ratios. As a result, the total-to-total efficiency was affected. Table 5 tabulates the mass-averaged changes in efficiency for 1.00, 1.25, and 1.50 percent relative cooling flow.

Radial cooling showed irregular changes in total-to-total efficiency. The changes in total-to-total efficiency due to radial cooling are shown in Figs. 14, 15, and 16. The passage-averaged efficiency change depended on the amount of coolant injection. For 1 percent coolant flow, the change was positive; at 1.25 percent the change was negative and at 1.5 percent the change was positive again. The mainstream pressure gradient turns the radial flow into the axial direction through a complex three-dimensional mix-

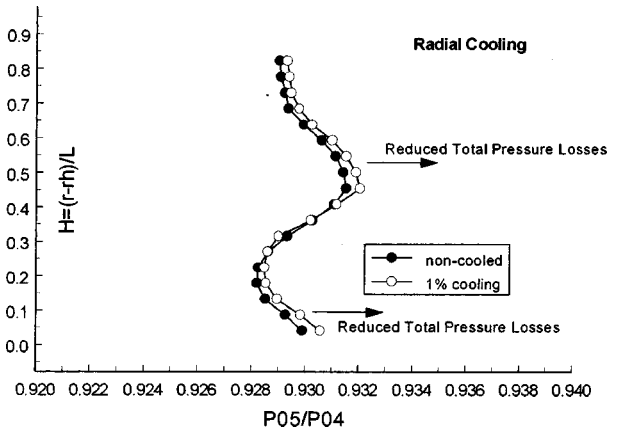

Fig. 15 Change in total pressure ratio (P_{05}/P_{04}) due to 1 percent radial cooling

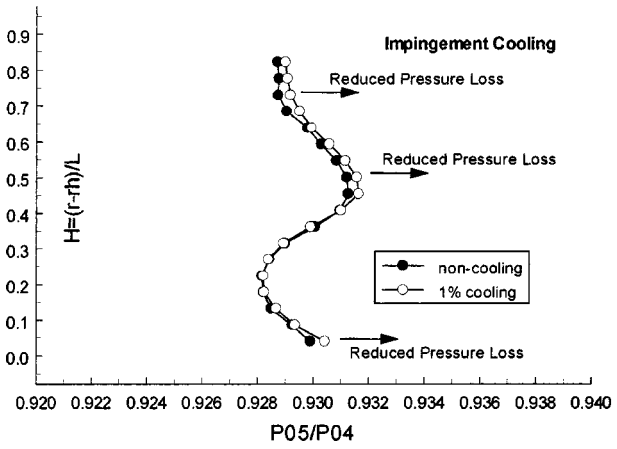

Fig. 18 Change in total pressure ratio (P_{05}/P_{04}) due to 1 percent impingement cooling

ing process. Different flow rates will cause possible separation of the mainstream flow and varying degrees of turbulent kinetic energy production and dissipation.

Impingement cooling caused the passage-averaged total-to-total efficiency to be lower. The results for the case of impingement cooling are given in Figs. 17, 18, and 19. The amount of change depended on the amount of cooling. The higher the flow rates, the less efficiency was lost. Over much of the passage the total pressure ratio was reduced, indicating lower pressure drop. In the midspan the total temperature ratio was increased leading to an increase in efficiency. However, the total temperature ratio was reduced over the hub and tip regions resulting in a lower efficiency. Very little useful energy is added to the flow through impingement cooling. Momentum is lost and the total temperature is increased when the fluid is stagnated on the rotor disk. The impingement cooling will tend to thicken the boundary layer with low-momentum fluid at a slightly elevated temperature. Increased total temperature, turbulent kinetic energy, and viscous dissipation in the boundary layer will lead to lower efficiency numbers.

Overall root injection results presented in Figs. 20, 21, and 22 showed the strongest changes in total-to-total efficiency. The passage averaged efficiency increase was over 1.5 percent for 1 percent coolant injection. The total pressure ratio was significantly increased over $H=0.1$ to $H=0.5$. This in conjunction with a decrease in total temperature ratio over $H=0.2$ to $H=0.55$ cause the efficiency to rise significantly. The efficiency increase is localized to the midspan region of the blade. At both the hub and tip the efficiency is slightly lower. The root injection energizes the nozzle wake and boundary layer near the hub wall. With an injection hole size on the order of the trailing edge thickness and with the injection inclined at 45 deg to the hub wall, the root injection can significantly energize the wake region. The mean velocity gradients are reduced through midspan, thereby reducing turbulent

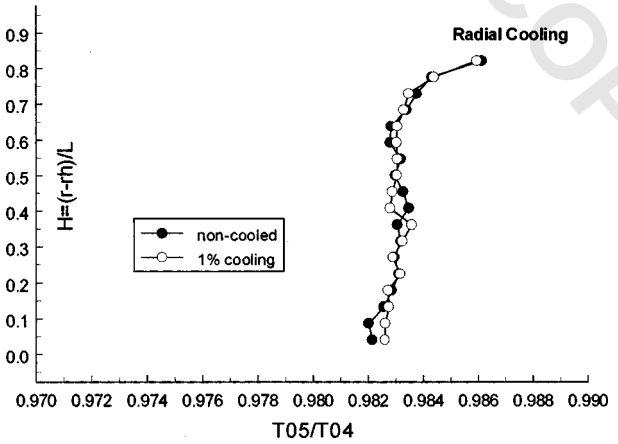

Fig. 16 Change in total temperature ratio (T_{05}/T_{04}) due to 1 percent radial cooling

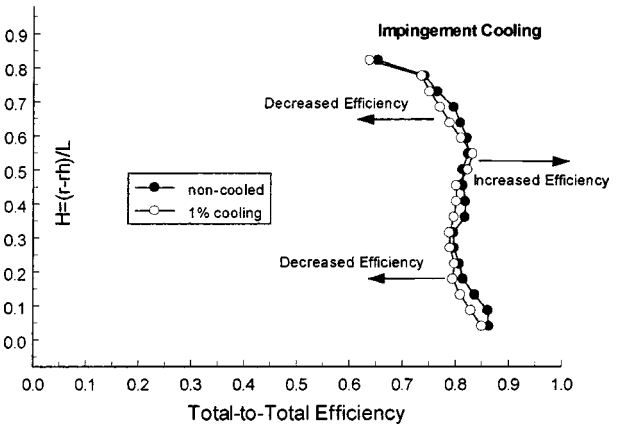

Fig. 17 Change in total-to-total efficiency (η) due to 1 percent impingement cooling

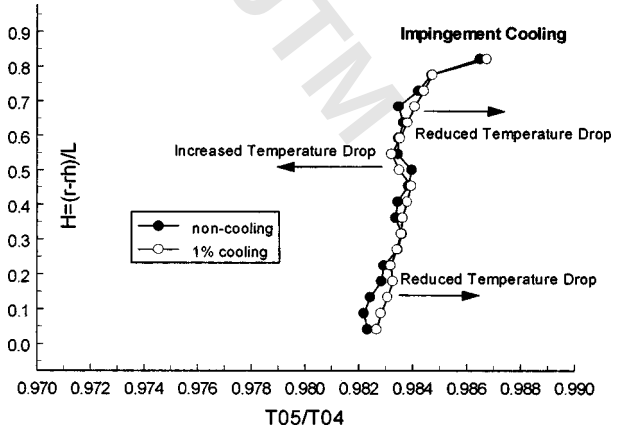

Fig. 19 Change in total temperature ratio (T_{05}/T_{04}) due to 1 percent impingement cooling

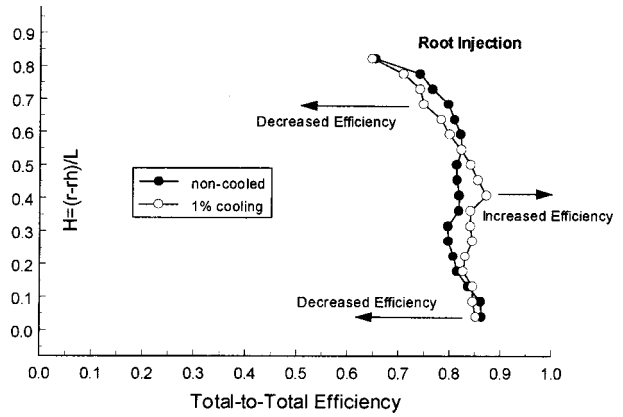

Fig. 20 Change in total-to-total efficiency (η) due to 1 percent root injection

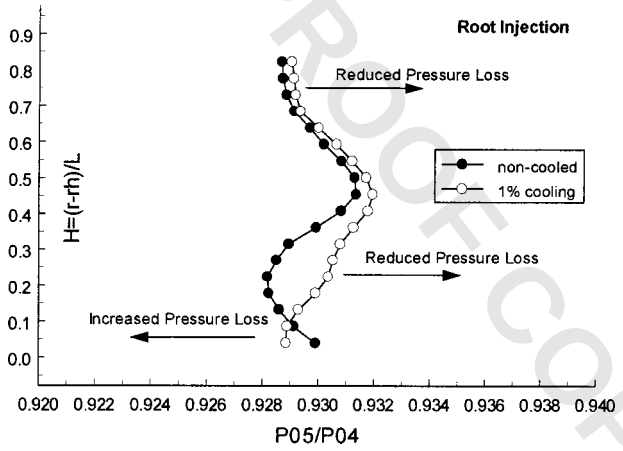

Fig. 21 Change in total pressure ratio (P_{05}/P_{04}) due to 1 percent root injection

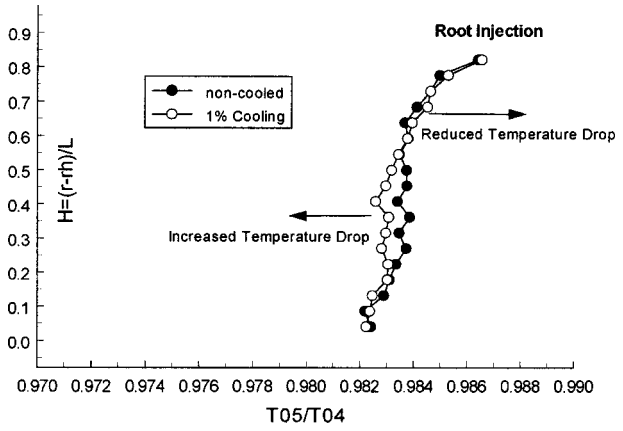

Fig. 22 Change in total temperature ratio (T_{05}/T_{04}) due to 1 percent root injection

mixing. Lower amount of turbulent mixing translates into less conversion of mean kinetic energy into internal energy via viscous dissipation.

Uncertainty Analysis

It was desired to both correct for quantifiable bias errors and to compute measurement uncertainties. The measurement philosophy of Wiedner [19] was adopted for the current research program. The philosophy is as follows:

Table 7 Absolute loading coefficient uncertainty

Parameter	Bias Error (B_x)	Effect on Loading Coefficient (ψ)
ρ	2.0%	1.96%
U_m	0.4%	0.80%
$P_{04} - P_{05}$	0.2%	0.2%

Table 8 Relative loading coefficient uncertainty

Parameter	Precision Error (S_x)	Effect on Loading Coefficient (ψ)
ρ	0.16%	0.16%
U_m	0.08%	0.15%
$P_{04} - P_{05}$	0.015%	0.015%

Table 9 Absolute efficiency uncertainty

Parameter	Bias Error (B_x)	Effect on Efficiency (η)
T_{04}	0.25 K	4.6%
T_{05}	0.25 K	4.7%
T_{0C}	0.25 K	0.005%
m_p	2.7%	0.005%
m_c	5.0%	0.01%
P_{04}	0.2%	0.21%
P_{05}	0.2%	0.21%

- When known sources of measurement error exist, avoid them.
- If known sources of error can not be avoided, and IF a repeatable bias error exists, correct for it.
- Avoid as many error sources as possible through calibration.
- If a source of error cannot be nulled thorough calibration or correction, provide an estimate of its magnitude.

Uncertainty in Fundamental Quantities. The five-hole and Kiel probe measurements were prone to various sources of error. They included turbulence effects, Reynolds number effects, Mach number effects, gradient effects, wall vicinity effects, probe blockage effects, recovery factor, misalignment errors, interpolation errors, calibration errors, data acquisition errors, and spatial location errors. Many of these error sources were quantifiable and were corrected for. The five-hole and Kiel probes were used to measure the fundamental quantities of u, v, w, P_o, P_s, and T_o. Following the methodology of Abernethy et al. [22], the uncorrectable uncertainty in velocity, pressure, and temperature and density are shown in Table 6.

It can be seen that there are significant differences between the precision (S_x) and bias errors (B_x). This is due to the interlaced manner in which the data sets were taken. In the present study it was desired to reduce the precision errors.

Following the error estimation of the five-hole probe and Kiel probe, the errors in the turbine performance parameters could be estimated. The ASME standard measurement uncertainty methodology [22] was used in conjunction with perturbation analysis to determine the measurement uncertainty.

Uncertainty in Loading Coefficient. The errors for the loading coefficient and change in loading coefficient are summarized in Tables 7 and 8. Combining the errors in Table 7 yields an uncertainty of 2.12 percent. The errors for the static pressure loss coefficient are identical to the loading coefficient. Combining the errors in Table 8 yields an uncertainty of 0.22 percent. The errors for the static pressure loss coefficient are identical to the loading coefficient.

Uncertainty in Total-to-Total Efficiency. The errors for the efficiency parameters are summarized in Tables 9 and 10. Combining the errors in Table 9 yields an efficiency error of 6.58

PROOF COPY 003104JTM

Table 10 Relative efficiency uncertainty

Parameter	Precision Error (S_x)	Effect on Efficiency (η)
T_{04}	0.1 K	1.8%
T_{05}	0.1 K	1.8%
T_{0C}	0.1 K	0.002%
m_p	0.44%	0.00087%
m_c	1.0%	0.002%
P_{04}	0.015%	0.02%
P_{05}	0.015%	0.02%

Table 11 Uncertainty summary

	Absolute Error (B_{xi})	Relative Error (S_{xi})	Relative with Circumferential Average (S_{xn}), n = 16	Relative with Passage Averaged (S_{xn}), n = 336
u, v, w	1.9%	0.4%	0.3%	0.065%
To, Ps	0.2%	0.015%	0.011%	0.0025%
To	0.25 K	0.1 K	0.075 K	0.016 K
ψ	2.12%	0.22%	0.17%	0.036%
η	6.58%	2.55%	1.91%	0.42%

percent. The errors for temperature measurement dominate. Combining the errors in Table 10 yields a relative efficiency error of 2.55 percent. The errors for temperature measurement dominate.

Uncertainty Summary. Table 11 summarizes the measured quantities and their respective uncertainties. The relationship in Eq. (4) was used to determine the uncertainty in an averaged quantity. It can be seen that the errors can be improved using circumferential and passage averaging on point quantities. This is useful, as most of the variations due to cooling are quite small and would be lost in the uncertainty variations otherwise.

$$S_{xn} = \frac{tS_{xi}}{\sqrt{n}} \tag{4}$$

Conclusions

The wheelspace coolant mixes with the mainstream flow and produces measurable changes in loss coefficient, velocity field, exit angle, and total-to-total efficiency. Local changes can be significant. The wheelspace coolant should not be neglected on the aerodynamic analysis of turbine blade stages. Overall, root injections showed the strongest effects although radial and impingement cooling showed measurable changes in loss coefficient, velocity, and efficiency.

The cooling flow caused significant local perturbations in the pressure coefficients. Root injection showed the largest changes, followed by radial cooling, and impingement cooling. In all cases, the strongest effects were below midspan but dwindling effects exist out to the tip regions. All three cooling methods caused significant local changes and a general redistribution of the data over the entire passage in both radial and tangential directions. Maximum effects ranged from 1.70, 0.86, and 2.57 percent for radial cooling, impingement cooling, and root injection, respectively. Although, the local perturbations were quite high, when passage-averaged data were evaluated, the changes were found to be small for radial cooling and impingement cooling. Root injection was able to affect the overall pressure coefficient as well as cause a redistribution of pressure coefficient data. The amount of change was almost five times that of impingement cooling and 30 times that of radial cooling.

The cooling flow was responsible for modifying the velocity profiles. Radial cooling and impingement cooling shifted the velocity profiles radially outward, while root injection was able to decrease the overturning and underturning. The point of maximum overturning was shifted radially by 10 percent for radial cooling and 5 percent for impingement cooling. The radial cooling is injected normal to the mainstream flow and would energize and thicken the rotor inlet boundary layer more than impingement cooling. The thicker boundary layer displaces the core flow and the passage vortex toward the tip region.

The root injection shows the most significant effects due to the coolant injection and is fundamentally different from radial cooling and impingement cooling. Root injection has the ability to affect the magnitude of the overturning and underturning. The amount of overturning and underturning is reduced.

Overall root injection showed the strongest changes in total-to-total efficiency. The passage-averaged efficiency increase was over 1.5 percent for root injection. The root injection efficiency increase was localized to the midspan region of the blade. With an injection hole size on the order of the trailing edge thickness and with the injection inclined at 45 deg to the hub wall, the root injection can significantly energize the nozzle wake region. Radial cooling showed irregular changes in total-to-total efficiency. For 1 percent coolant flow the change was positive, at 1.25 percent the change was negative and at 1.5 percent the change was positive again. Impingement cooling caused the passage-averaged total-to-total efficiency to drop.

Acknowledgments

This paper is based on university research funded by the U.S. Dept. of Energy, AGTSR program. The authors would like to acknowledge Drs. L. Golan, D. Fant, and R. Wenglarz as program monitors.

Nomenclature

A = exit area of single cooling hole
b = $\rho_C U_C / \rho_P U_P$
c_p = specific heat
H = normalized radial position $= (r - r_h)/L$
h = entropy
L = rotor blade height
R = gas constant
m = mass flow rate
M = Mach number $= U/\sqrt{\gamma RT}$
n = number of cooling holes (23)
P = pressure
r = radial position
T = temperature
u = axial velocity component
U, V, W = wheel speed, relative velocity, absolute velocity
U_d = discharge velocity $= m_C / n\rho A$
v = radial velocity component
w = tangential velocity component
α = pitch angle, exit flow angle inclined to the turbine axis
β = yaw angle, exit flow angle
γ = ratio of specific heats
η = efficiency
ρ = density
Θ = angle in circumferential direction

Subscripts

o = total condition
04 = entry of nozzle condition
05 = exit of rotor condition
1, 2, 3, 4, 5 = five-hole probe hole designation
c = cooling
h = hub
m = midspan condition
p = primary or mainstream
s = static condition
tt = total-to-total

References

[1] Karstensen, K., 1997, ''The Solar Turbines Project—Developing the 21st Century Gas Turbine,'' Department of Energy Office of Fossil Energy, Project Synopsis.

[2] Alwang, A., 1981, ''Measurement of Non-Steady Fluid Dynamic Quantitiés,'' von Karman Institute for Fluid Dynamics Lecture Series—Measurement Techniques in Turbomachines.

[3] Metzger, D., Kim, Y., and Yu, Y., 1993, ''Turbine Cooling: An Overview of some Focus Topics,'' *Proc. 1993 International Symposium on Transport Phenomena in Thermal Engineering.*

[4] Owen, J. M., and Rogers, R. H., 1989, ''Flow and Heat Transfer in Rotating Disc Systems, Vol. 1: Rotor-Stator Systems,'' Research Studies Press ltd. and John Wiley.

[5] Bunker, R., Metzger, D., and Wittig, S., 1992, ''Local Heat Transfer in Turbine Disk Cavities: Part I—Rotor and Stator Cooling With Hub Injection of Coolant,'' ASME J. Turbomach., **114**, pp. ■.

[6] Bunker, R., Metzger, D., and Wittig, S., 1992, ''Local Heat Transfer in Turbine Disk Cavities: Part II—Rotor Cooling With Radial Location Injection of Coolant,'' ASME J. Turbomach., **114**, pp. ■.

[7] von Karman, T., 1921, ''Über Llaminare und Turbulente Reibung,'' Z. Angew. Math. Mech., **1**, pp. ■.

[8] Cobb, E., and Saunders, O., 1956, ''Heat Transfer From a Rotating Disk,'' Proc. R. Soc. London, Ser. A, **26A**, pp. 343–351.

[9] Maroti, L., Deak, G., and Kreith, F., 1960, ''Flow Phenomena of Partially Enclosed Rotating Disks,'' ASME J. Basic Eng., **82**, pp. ■.

[10] Daily, J., and Nece, R., 1960, ''Chamber Dimensional Effects on Induced Flow and Frictional Resistance of Enclosed Rotating Disks,'' ASME J. Basic Eng., **82**, pp. 217–232.

[11] Dorfman, L. A., 1963, *Hydrodynamic Resistance and the Heat Loss of Rotating Solids*, Oliver and Boyd, Edinburgh.

[12] Metzger, D., Mathis, W., and Grochowsky, L., 1979, ''Jet Cooling at the Rim of a Rotating Disk,'' ASME J. Eng. Power, **101**, pp. 68–72.

[13] Popiel, C., and Boguslawski, L., 1986, ''Local Heat Transfer From a Rotating Disk in an Impinging Round Jet,'' ASME J. Heat Transfer, **108**, pp. 357–364.

[14] Qureshi, G., Nguyen, M., Saad, N., and Tadros, R., 1989, ''Heat Transfer Measurements for Rotating Turbine Disks,'' ASME Paper No. 89-GT-26.

[15] Pincombe, J., 1989, ''Chapter 33, Gas Turbine Disk Cooling Flows,'' *Handbook of Flow Visualization*, Wen-Jei Yang, ed., Hemisphere Publishing Corp.

[16] Lakshminarayana, B., Camci, C., Halliwell, I., and Zaccaria, M., 1996, ''Design and Development of a Turbine Research Facility to Study Rotor-Stator Interaction,'' Int. J. Turbo Jet Engines, **13**, pp. 155–172.

[17] Laksminarayana, B., Camci, C., Halliwell, I., and Zaccaria, M., 1992, ''Investigation of Three Dimensional Flow Field in a Turbine Including Rotor/Stator Interaction,'' AIAA/SAE/ASME/ASEE 28th Joint Propulsion Conference and Exhibit, July 6–8, Nashville, TN.

[18] Friedrichs, S., Hodson, H. P., and Dawes, W. N., 1997, ''Aerodynamic Aspects of Endwall Film-Cooling,'' ASME J. Turbomach., **119**, pp. 786–795.

[19] Wiedner, G., 1994, ''Passage Flow Structure and its Influence on Endwall Heat Transfer in a 90° Turning Duct,'' Ph.D. Thesis in Aerospace Engineering, The Pennsylvania State University.

[20] Zaccaria, M. A., 1994, ''Investigation of Three Dimensional Flow Field in a Turbine Including Rotor/Stator Interaction,'' Ph.D. Thesis in Aerospace Engineering, The Pennsylvania State University.

[21] McDonel, J. D., and Eiswerth, J. E., 1977, ''Effects of Film Injection on Performance of a Cooled Turbine,'' AGARD Conference Proceedings, CP-229.

[22] Abernathy, R. B., Benedict, R. P., and Dowdell, R. B., 1985, ''ASME Measurement Uncertainty,'' ASME J. Fluids Eng., **107**, pp. ■.